Draft version November 8, 2016
Preprint typeset using LaTeX style AASTeX6 v. 1.0

arXiv:1611.02182v1 [astro-ph.GA] 7 Nov 2016

DIFFUSION AND CLUSTERING OF CARBON DIOXIDE ON NON-POROUS AMORPHOUS SOLID WATER

Jiao He[1] and Shahnewaj M. Emtiaz and Gianfranco Vidali[2]
Physics Department, Syracuse University, Syracuse, NY 13244, USA

[1]jhe08@syr.edu
[2]gvidali@syr.edu

ABSTRACT

Observations by ISO and Spitzer towards young stellar objects (YSOs) showed that CO_2 segregates in the icy mantles covering dust grains. Thermal processing of ice mixture was proposed as responsible for the segregation. Although several laboratory studied thermally induced segregation, a satisfying quantification is still missing. We propose that the diffusion of CO_2 along pores inside water ice is the key to quantify segregation. We combined Temperature Programmed Desorption (TPD) and Reflection Absorption InfraRed Spectroscopy (RAIRS) to study how CO_2 molecules interact on a non-porous amorphous solid water (np-ASW) surface. We found that CO_2 diffuses significantly on a np-ASW surface above 65 K and clusters are formed at well below one monolayer. A simple rate equation simulation finds that the diffusion energy barrier of CO_2 on np-ASW is 2150±50 K, assuming a diffusion pre-exponential factor of 10^{12} s^{-1}. This energy should also apply to the diffusion of CO_2 on wall of pores. The binding energy of CO_2 from CO_2 clusters and CO_2 from H_2O ice have been found to be 2415 ± 20 and 2250 ± 20 K, respectively, assuming the same prefactor for desorption. CO_2-CO_2 interaction is stronger than CO_2-H_2O interaction, in agreement with the experimental finding that CO_2 does not wet np-ASW surface. For comparison, we carried out similar experiments with CO on np-ASW, and found that the CO-CO interaction is always weaker than CO-H_2O. As a result, CO wets np-ASW surface. This study should be of help to uncover the thermal history of CO_2 on the icy mantles of dust grains.

Keywords: astrochemistry — ISM: molecules — methods: laboratory: solid state — methods: laboratory: molecular — dense matter

1. INTRODUCTION

CO_2 constitutes a significant fraction of ices coating dust grains in interstellar clouds, with CO_2 abundance ranging between 15% and 40%. Other major ice components include water, the most abundant, and CO and CH_3OH (Pontoppidan et al. 2008; Boogert et al. 2015). Through observations of solid state of CO_2 and CO IR features a picture of the state and history of the cloud (Nummelin et al. 2001; Whittet et al. 1998, 2007, 2009; Boogert et al. 2015; Cook et al. 2011) can be obtained. By analyzing the double-peak feature of CO_2 bending mode at 660 cm^{-1}, CO_2 in the pure form has been found by ISO (Gerakines et al. 1999) and Spitzer (Pontoppidan et al. 2008) towards young stellar objects (YSOs). The fact that this double-peak feature is only observed toward regions where the protostar has already "turned on" (see Öberg et al. (2009); Pontoppidan et al. (2008); Boogert et al. (2015) and references therein) suggests that the segregation of CO_2 is induced by thermal processing of the ice mixture. To explain these observations and characterize the segregation of CO_2 in ices, the following three mechanisms are possible: (a) collapse of the porous ice structure that causes CO_2 molecules to move and get trapped in pockets of high CO_2 concentration; (b) penetration of CO_2 molecules through bulk non-porous amorphous solid water ice (np-ASW) by diffusion; (c) diffusion of CO_2 along the wall of pore surfaces. The first one requires highly porous structure and relatively high concentration of CO_2 with respect to water, a scenario not yet confirmed by observations (Keane et al. 2001). The second one requires a low energy barrier for diffusion in the bulk, but experiments show otherwise (Öberg et al. 2009; Mispelaer et al. 2013). The third one — diffusion along the surfaces of the walls of ice — is the most probable mechanism for CO_2 segregation, and is the focus of this study.

There have been several laboratory works that studied mid-IR features of CO_2, i.e., the bending mode ν_2 at 660 cm^{-1} and the asymmetric stretch band ν_3

at $\sim$ 2340 cm^{-1} and near-IR overtones and combination bands (Ehrenfreund et al. 1998; Dartois et al. 1999; Baratta et al. 2000; Palumbo & Baratta 2000; Bernstein et al. 2005; Hodyss et al. 2008; Öberg et al. 2009; Isokoski et al. 2014). Studies of CO_2:H_2O binary and CO_2:H_2O:CH_3OH ternary ices have found that segregation becomes significant above 50–60 K and up to 85 K (Ehrenfreund et al. 1998; Palumbo & Baratta 2000; Bernstein et al. 2005; Hodyss et al. 2008), although quantitative values so obtained differ among these measurements (these temperature values refer to laboratory experimental conditions; in space they would be lower, see below). Palumbo & Baratta (2000) studied the dependence of the mixing ratio CO_2:H_2O on segregation, and found that below 10% CO_2 in H_2O there is no segregation of CO_2. Öberg et al. (2009) did a comprehensive study of segregation in binary mixtures (CO_2:H_2O); they found a thickness as well as a composition dependence. Coupling data with a Monte Carlo simulation, they reported an energy barrier of 1080 $\pm$ 190 K for segregation of CO_2 at the surface of the ice. Isokoski et al. (2014) studied segregation of CO_2 in H_2O using the combination bands $\nu_1 + \nu_3$ at 3704 cm^{-1} and $2\nu_2 + \nu_3$ at 3597 cm^{-1} which are sensitive to the local environment (Keane et al. 2001). Their study, which explored the influence of morphology of the ice, showed that high porosity facilitates CO_2 segregation. Indeed this and other studies suggest the link between diffusion of CO_2 molecules on the surface of ice and segregation. The work presented here addresses this issue in a quantitative way.

Surface diffusion of CO_2 on ice (whether on pores or at the interface between the ice surface and vacuum) is much faster than *through* ice (Öberg et al. 2009); thus, recent studies were concentrated on studying diffusion and aggregation on the surface of water ice. Ghesquière et al. (2015) studied in the laboratory the diffusion of CO_2 through compact ASW, but in the experiments the ice was deposited at 80 K, which may not be high enough to be truly compact. On the contrary, our laboratory measurements show no evidence of CO_2 penetration into np-ASW deposited at 130 K. Another important factor for the formation of CO_2 clusters is the binding energy of CO_2 from CO_2 clusters and CO_2 from water ice surface. Clusters can be formed only when the binding energy of CO_2 from CO_2 clusters is stronger than that of CO_2 from water ice surface. To study the binding energies, Noble et al. (2012) used temperature programmed desorption (TPD) to measure the TPD of CO_2 on a np-ASW surface down to 0.5 monolayer (ML) coverage; based on the argument that CO_2 interaction energy with the water ice surface is stronger than the interaction energy at monolayer coverage, they argued for non-wetting. However, the measurement at 0.5 ML coverage is not low enough to study the onset of segregation or cluster formation (see below); therefore the behavior of CO_2 at lower coverages is unknown. Karssemeijer et al. (2014) used molecular dynamics simulation with a new ab initio calculation of the interaction energy of CO_2-H_2O and CO_2-CO_2 in the gas phase and on water ice. They found that in the gas phase the CO_2-H_2O interaction strength is twice as the CO_2-CO_2, while in the solid state the difference between them is much smaller. The result of their molecular dynamics simulations found no indication of island formation or clustering during deposition of CO_2 on water ice. Because the simulation occurs on time scales orders of magnitude faster than an actual deposition, some caution should be exercised in applying these results.

To resolve this issue and obtain information of how CO_2 molecules diffuse on water ice, as well as the binding energies, we used a combination of TPD and RAIRS techniques to study systematically the interaction of CO_2 with np-ASW. For comparison purposes, some of the experiments were also done with CO. We explored both the temperature and coverage dependence of CO_2 clustering on np-ASW, and found how the diffusion rate determines the clustering of CO_2. An estimate of the energy barrier to diffusion of CO_2 molecules on water ice is also obtained. Technical improvements allowed us to study the CO_2-H_2O system down to $\sim$ 1% ML coverage of CO_2. This is an important step that allows us to better approximate the conditions of the experiment to the conditions in the ISM. By choosing a np-ASW ice, we single out the interaction between CO_2 and the surface of water, and we avoid the complication of the structural changes of porous ice and of the trapping of CO_2 in pores that affect the segregation rate. However, our results should be translatable to more porous ice surfaces.

The remainder of the paper is organized as below: in Section 2 we describe briefly the experimental setup and how ices are grown and characterized; Section 3 presents the results and analysis, followed by a discussion of the astrophysical implications in Section 4.

2. EXPERIMENTAL SETUP

Experiments were carried out in an ultra-high vacuum (UHV) chamber connected to two molecular beam lines. The pressure in the UHV chamber reaches 1×10^{-10} torr after bake-out. Ices are grown on a gold coated copper disk located at the center of the UHV chamber. The sample disk can be cooled by liquid helium to $\sim$ 8 K and heated up to 450 K by a resistive heater. The temperature of the sample disk was measured by a calibrated silicon diode (Lakeshore DT 670) and controlled by a Lakeshore 336 temperature controller with an uncertainty of less than 50 mK. A Hiden Analytical

quadrupole mass spectrometer (QMS) was mounted on a rotatable flange that can be used to measure the intensity of the incoming molecular beam or the molecules desorbing from the sample in Temperature Programmed Desorption (TPD) experiments. A Nicolet 6700 Fourier Transform Infrared (FTIR) spectrometer in Reflection Absorption InfraRed Spectroscopy (RAIRS) setup was used to monitor ices grown on the substrate. The infrared beam was focused by an off-axis paraboloidal mirror before entering the chamber through a differentially pumped KBr window. It is then reflected from the sample at 78° incidence angle and exits the chamber through another KBr window,; it is then focused by an off-axis ellipsoidal mirror before entering a MCT-B detector with a working range from 650 to 4000 cm^{-1}. For experiments carried out in this work, the highest resolution 1 cm^{-1} was used. Spectra were collected by averaging 22–23 scans every 30 seconds.

Water ice was grown by vapor deposition from the background using a capillary array (He et al. 2016a). The capillary array is facing empty space in the chamber for background deposition onto the substrate. A nude ionization pressure gauge was used to monitor the pressure in the chamber. We assume that during background deposition, the pressure readout from the pressure gauge is the same as that close to the substrate. Distilled water was used for water deposition. It went through at least three freeze-pump-thaw cycles before being introduced into the chamber. In this work we mostly use non-porous amorphous solid water (np-ASW), which was grown by background deposition of water vapor when the substrate was at 130 K. After deposition, the ice remained at 130 K for 20 minutes to stabilize the ice structure before cooling down for further experiments. CO_2 ice was grown either by deposition from the molecular beam or by background deposition from the capillary array. The thickness of CO_2 ice grown from background deposition was calculated by integrating the chamber pressure over time. The ion gauge correction for different gases was taken into account. The recording of the pressure in the chamber and the calculation of the thickness (in Langmuir) in real time were handled by a LabVIEW program. This ensures that the thickness of deposition can be controlled accurately within an uncertainty of 3%. Unity sticking is assumed for all of the experiments in this work, and this is supported by previous sticking measurement by our group (He et al. 2016b). At room temperature (∼294 K), 1 Langmuir (1L= 1×10^{-6} torr·s) of H_2O, CO, and CO_2 amounts to 5.23×10^{14}, 4.19×10^{14}, and 3.34×10^{14} molecules cm^{-2}, respectively — see the Appendix for details. The column density of CO_2 in units of L can be converted to thickness as 1 L=1.9Å, assuming a CO_2 density of 1.28 g·cm^{-3} (Gerakines & Hudson 2015). From CO TPD spectra in Section 3 we show that 1 L of CO corresponds to about 1 monolayer (ML) coverage on np-ASW. We assume that the number of CO_2 molecules in 1 ML coverage is the same as that of CO, and in the remaining part of this work we use L and ML interchangeably for both CO_2 and CO.

Details of the molecular beam can be found in a previous publication (He et al. 2016b). The deposition rate from the beam was controlled by an Alicat MCS-5 mass flow controller with a relative uncertainty of less than 1%. The beam deposition time was automated using a computer controlled flag with an accuracy down to ∼50 ms. The molecular beam is at 8° with respect to surface normal, and covers most of the sample surface area, which is 1 cm^2. Because the infrared beam does not overlap perfectly with the molecular beam on the sample, the calibration of thickness needs special attention. Usually the ice thickness can be calculated by integrating the absorption of a known absorption band and comparing it with the absorption intensity found in the literature. But this method does not apply here, because the molecular beam covers a smaller area than the infrared beam. We instead compared the infrared spectrum of CO_2 from beam deposition and from background deposition on annealed water ice to calibrate the beam deposition rate/beam flux. More details of the calibration is in the Appendix.

3. RESULTS AND ANALYSIS

In the first experiment, CO_2 was deposited from the beam onto the np-ASW ice at 10 K. Infrared spectra were recorded during deposition, see Figure 1. At very low dose, CO_2 molecules are isolated on the surface and interact primarily with the water surface, as indicated by the asymmetrical stretch ν_3 absorption peak at 2347 cm^{-1}. As the CO_2 concentration increases, CO_2 molecules interact primarily among themselves in clusters. In the RAIRS geometry of absorption and reflection at glancing angle, solid state CO_2 aggregates are characterized by a peak at ∼ 2380 cm^{-1} (Escribano et al. 2013; Edridge et al. 2013) due to the LO phonon mode (Berreman 1963). Also shown in Figure 1 is the integrated area of ν_3 band, which is linear with deposition dose, regardless of the peak shape and position.

In the second experiment, 0.23 L of CO_2 was deposited from the beam at a rate of 0.35 L·$minute^{-1}$ on np-ASW surface at 10 K, and it was followed by a linear increase of the temperature at 2 K·$minute^{-1}$. Figure 2 shows the spectra of ν_3 band during heating. Compared with Öberg et al. (2009)'s and Noble et al. (2012)'s work, we focus on a much lower surface coverage of CO_2 in order to find the temperature at which CO_2 starts to diffuse on the surface. At low temperature and low surface cov-

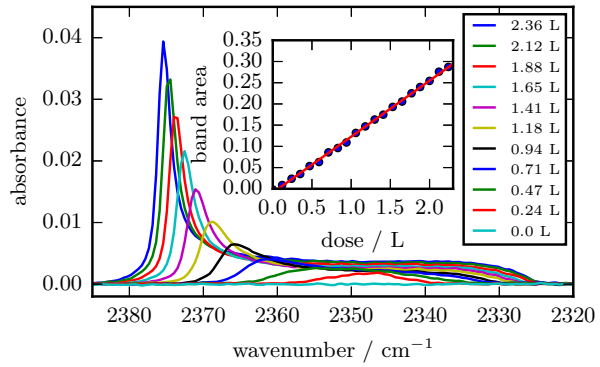

Figure 1. CO_2 ν_3 band during deposition of CO_2 on np-ASW at 10 K. The integrated band area versus deposition dose is shown in the center inset. The deposition dose for each curve is in the right side inset.

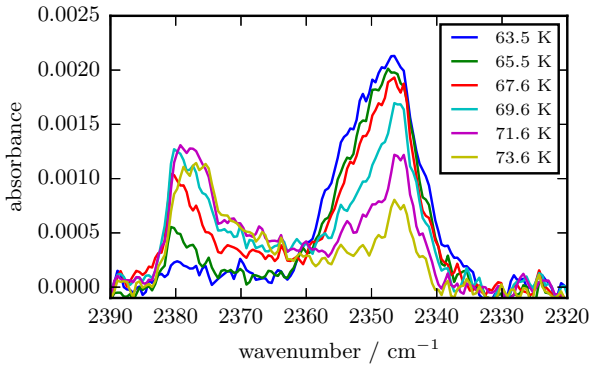

Figure 2. CO_2 ν_3 band during heating in the following experiment: 0.23 L of CO_2 was deposited from the beam onto np-ASW at 10 K, followed by heating at 2 K/minute. Surface temperature is shown in the inset.

erage, the isolated CO_2 molecules have an absorption band at around 2347 cm^{-1}. As the sample is heated to ∼65 K, the band at 2347 cm^{-1} decreases and another band emerges at ∼2380 cm^{-1}, which is associated with aggregated CO_2. This indicates that at ∼65 K, the diffusion rate of CO_2 on np-ASW becomes significant and CO_2 molecules are able to move around and form clusters. The IR spectrum therefore shows a decrease in the band of CO_2-water interaction and an increase in the one of CO_2-CO_2 interaction. From this experiment we found that in the laboratory time scale, the ice temperature needs to be close to or higher than 65 K for CO_2 segregation/clustering to happen.

Clustering behavior of CO_2 also depends on surface coverage. The more CO_2 is on the surface, the easier is to form clusters. At a given temperature, there exists a threshold coverage above which CO_2 forms clusters. We carried out the following experiment to find out the clustering threshold at 65 K. With np-ASW at 65 K we deposited CO_2 continuously at a rate of 0.035 L·minute^{-1} and monitored the IR spectrum. At this surface temperature CO_2 should be mostly mobile. Figure 3 shows

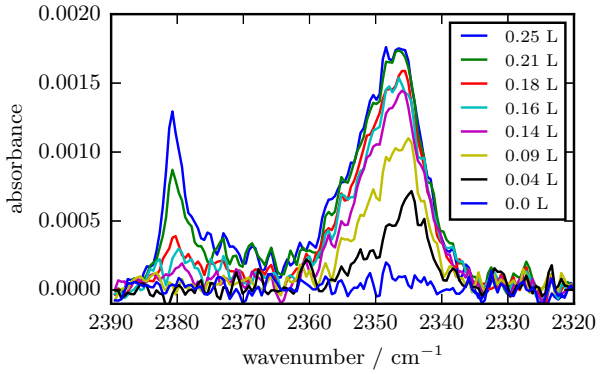

Figure 3. CO_2 ν_3 band during deposition of CO_2 from the beam onto a np-ASW at 65 K. The deposition dose is shown in the inset.

that there is only one peak at 2347 cm^{-1} below ∼0.17 L, while at and above ∼0.17 L the peak at 2380 cm^{-1} begins to emerge. Therefore 0.17 L is the clustering threshold at 65 K. The existence of a coverage threshold for clustering is consistent with Palumbo & Baratta (2000), which found a concentration threshold of 10% for clustering. At higher surface temperature, the threshold can be lower.

Similar experiments were carried out for CO on np-ASW. Lauck et al. (2015) have already found that the diffusion of CO becomes significant at $>$ 15 K. We kept the np-ASW at 22 K, at which the diffusion is fast, while the desorption is still negligible (He et al. 2016a). Based on previous measurement from our group (He et al. 2016b), at 22 K the sticking of CO is unity. CO was deposited continuously from the beam at a rate of 0.035 L·minute^{-1}. The measured IR spectra are shown in Figure 4. Three different absorption bands can be seen in the figure, at 2140 cm^{-1}, 2142 cm^{-1}, and 2152 cm^{-1}. The assignment of these peaks are discussed extensively in Palumbo et al. (2006); Palumbo (2006); Cuppen et al. (2011). At low coverage there are only two peaks at 2140 cm^{-1} and 2152 cm^{-1}, growing linearly with coverage. The former has been seen towards numerous young stellar objects (Pontoppidan et al. 2003) and is due to the interaction of CO with non-dangling bond sites. The latter is due to CO interacting with dangling-bond (dOH) sites (Al-Halabi et al. 2004). After ∼0.6 L, the band at 2152 cm^{-1} saturates while the 2140 cm^{-1} peak continues to increase linearly until about 1.1±0.1 L, at which the peak at 2142 cm^{-1} due to pure CO (CO in CO environment) emerges. We used two Gaussian distributions to fit the components at 2152 and 2140 cm^{-1}, and one Lorentzian distribution to fit the component at 2142 cm^{-1} (He et al. 2016). The corresponding areas of these three components are shown in Figure 5.

For CO the critical coverage at which CO in the pure form emerges is at 1.1 ± 0.1 L, which is much higher

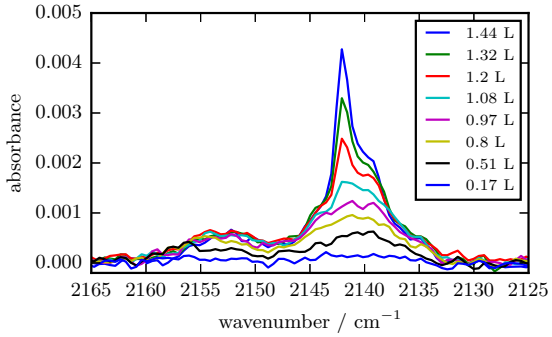

Figure 4. CO stretching band during deposition of CO from the beam on np-ASW at 22 K. The deposition dose is shown in the inset.

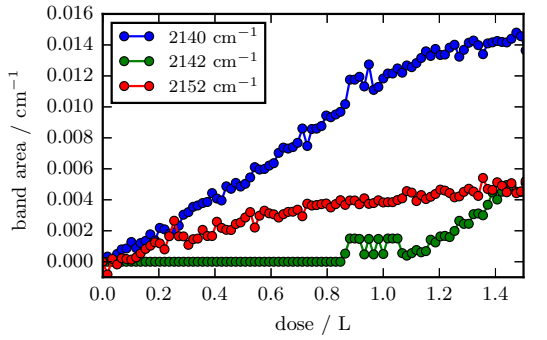

Figure 5. Band area versus deposition dose for the absorption peaks in Figure 4.

than that for CO_2. Later it will be shown that 1 L corresponds to 1 ML. This suggests that CO completely wets the surface before building up layers. The underlying reason is because the CO-CO interaction is weaker than the CO-water interaction. On the contrary, the CO_2-CO_2 interaction is stronger than the CO_2-water interaction and CO_2 forms clusters. This is a well-known case in thin film growth, also called Vollmer-Weber growth. On the other extreme of the adsorbate-adsorbate versus adsorbate-substrate interaction, growth occurs layer-by-layer. This is the so called Frank-van der Merwe growth (e.g. Ratsch & Venables 2003).

In surface science literature, one of the tools to study the formation of islands or clusters on a surface is TPD. TPD spectra are usually analyzed using the Polanyi-Wigner equation:

$$\frac{\mathrm{d}\theta(t)}{\mathrm{d}t} = -\nu\theta^n(t)\exp\left(-\frac{E_\mathrm{b}(\theta)}{k_\mathrm{B}T(t)}\right) \qquad (1)$$

where ν is the desorption pre-exponential factor (or prefactor). In this work we take the widely used value of 10^{12} s^{-1}. $\theta(t)$ is the coverage defined as percentage of a monolayer (ML), i.e., the number of adsorbate particles divided by the number of adsorption sites on the surface, n is the order of desorption, $E_\mathrm{b}(\theta)$ is the binding energy, which can depend on coverage, k_B is Boltzmann constant, $T(t)$ is the temperature of the surface. For $n = 0$, the desorption rate does not depend on the amount of material on the surface. Thus, this indicates desorption from multilayer films. $n = 0$ or close to it applies also in the desorption of clusters of particles on the surface. Zeroth order desorption is recognized by the fact that TPD traces of film with different values of the coverage have overlapping leading edges (Kolasinski 2008).

We carried out TPDs of both CO_2 and CO on np-ASW, see Figure 6 and 7, respectively. For CO_2, $^{13}CO_2$ was used to obtain higher signal-to-noise ratio. From here on the isotope label is dropped. In the TPD experiments for both CO and CO_2, the deposition rate is 0.70 L·minute^{-1}, and the heating ramp rate is 0.5 K·s^{-1}. These TPD spectra of CO_2 and CO are similar to our previous measurement (He et al. 2016a), except here the signal-to-noise ratio is better. The CO_2 TPDs here are for submonolayer coverage; for higher and multilayer coverage, see He et al. (2016a). In the case of CO on np-ASW at a coverage from zero to 0.7 L, the TPD traces show a similar shape and the peak temperature shifts to lower values with increasing deposition. This translates to a decrease in the binding energy with coverage. Between 0.7 L and 0.87 L, a second peak emerges, but it does not have the characteristics of zeroth order desorption yet, such as a common leading edge. At this point, the interaction of CO is with both H_2O and CO. Above 1.05 L, the peak at $\sim$ 30 K is due to the CO-CO interaction, as is evident from the common leading edge, indicating multilayer growth. In the submonolayer regime, trailing edges overlap, which indicates that CO occupies deep adsorption sites before shallow sites. We applied the same direct inversion procedure as in He et al. (2016a) to obtain the desorption energy distribution (not shown); we find that it is close to the distribution reported in He et al. (2016a). The binding energy of CO-CO (870 K) is located at or below the lower boundary of CO-H_2O binding energy (870–1600 K). At about 1.05 L zeroth order desorption is observed, which suggests that a multilayer CO is building up. This coincides with the infrared measurements shown in Figure 4. We define 1 ML coverage as the amount of CO molecules that fully covers the surface area on np-ASW, and in the case of CO on np-ASW 1 ML corresponds to 4.2×10^{14}molecules·cm^{-2} (see Section 2). This number may also be used for other molecules after taking into account the correction factor for the size of molecules.

In the CO_2 TPDs, from 0.01 L to 0.06 L there is only one peak centered at $\sim$76 K with small variation with coverage, which indicates first order desorption. At 0.12 L, a second peak at $\sim$ 84 K emerges and continues to grow as coverage increases. This second peak is due to the formation of CO_2 clusters. At coverage higher than 0.35 L, the first peak at 76 K begins to drop (see

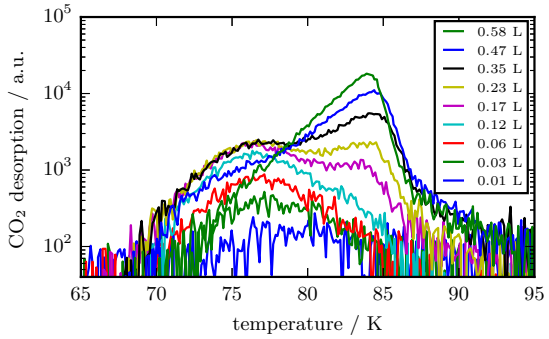

Figure 6. Temperature programmed desorption (TPD) spectra of $^{13}CO_2$ on np-ASW. The deposition dose is shown in the inset. $^{13}CO_2$ was deposited from the beam when the surface was at 50 K. The heating ramp rate during the TPD is 0.5 K/s.

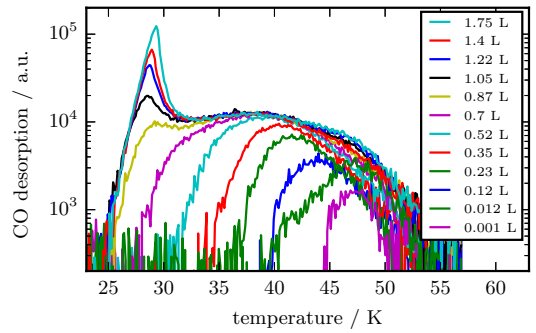

Figure 7. Same as in Figure 6 but for CO on np-ASW. CO was deposited from the beam when the surface was at 22 K.

traces at 0.47 L and 0.58 L). This is because at higher coverage, as CO_2 cluster formation begins, there is an decreasing number of isolated CO_2 molecules and an increasing number of CO_2 molecules in clusters. At even higher coverages, the TPD shows features of typical zeroth order desorption (He et al. 2016a).

To obtain CO_2-H_2O and CO_2-CO_2 interaction energies, we fitted the low coverage CO_2 TPDs in Figure 6 using two first order desorption peaks. Strictly speaking, the second peak due to CO_2 desorption from CO_2 clusters is not first order. But when the coverage is much lower than the coverage at which zero order desorption is significant, it is a good approximation. We only fit TPDs up to 0.23 L because at higher coverages the fitting is no longer satisfactory. The fitting result is shown in Figure 8. The best fitting energies are 2250 ± 20 K and 2415 ± 20 K for the first peak (CO_2-H_2O) and second peak (CO_2-CO_2), respectively. This CO_2-H_2O interaction energy value is comparable with the value of 2268 K on the same type of ice obtained by Noble et al. (2012). Figure 9 shows the area of the two peaks with coverage. The first peak for discrete CO_2 shows saturation after ~0.17 L. The second peak for clusters grows slowly at very low coverage and becomes faster when the first

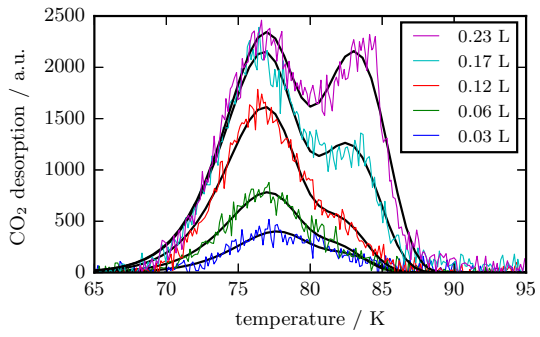

Figure 8. Fitting of selected TPD spectra in Figure 6 using two first order desorption peaks. The experimental data are shown in thin color lines and fitted curves in thick black lines.

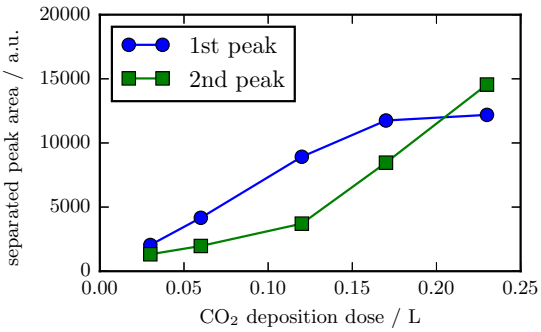

Figure 9. The area of the two TPD peaks obtained from the fitting shown in Figure 8. Lines are only to guide the eye.

peak saturates.

4. DISCUSSION AND ASTROPHYSICAL IMPLICATIONS

Following the observation of pure CO_2 in low mass young stellar objects (Pontoppidan et al. 2008), it has been proposed (Gerakines et al. 1999; Pontoppidan et al. 2008) that CO_2 could be used as a tracer of the temperature of the ice. Pontoppidan et al. (2008); Ioppolo et al. (2009, 2013) showed there are two ways to explain the aggregation of CO_2 in ices; it is either by segregation—which involves diffusion in the ice matrix, or by distillation, that is the sublimation of CO in CO-CO_2 mixed layers. Using the data of Ehrenfreund et al. (1999), they came up with an activation energy for segregation of 4900 K. In new IR studies of CO_2-water ice mixtures, Öberg et al. (2009) fitted the amount of segregated CO_2 as a function of time using an Arrhenius expression, finding an activation energy of 1080 ± 190 K and a pre-exponent of $2 \times 10^{5\pm1}$ for a H_2O:CO_2=2:1 mixture. The very high concentration of CO_2 prevents them to single out the effect of surface diffusion. Our investigation is instead centered on cluster formation at much lower concentration of CO_2 in water ice. Therefore, it complements the work of Öberg et al. (2009).

To extract the diffusion energy barrier $E_{\rm dif}$ for a single CO_2 molecule on the surface of np-ASW, we developed a simple rate equation model to simulate the formation of clusters. We assume that $E_{\rm dif}$ takes a single value instead of a continuous distribution. We assume that clusters do not diffuse. The rate equation deals only with diffusion and ignores desorption. Consequently, we only attemp to fit $T < 70$ K part of the experiment. The diffusion rate is expressed as:

$$D(t) = \nu \exp(-E_{\rm dif}/k_{\rm B}T(t)) \quad (2)$$

where ν is the pre-exponential factor for diffusion, which is assumed to be the same as desorption prefactor 10^{12} s^{-1}. This is a reasonable assumption considering that we describe the motion of a single small molecule largely unaffected by the presence of other CO_2 molecules. We denote $C_1(t)$ as the coverage of isolated CO_2 molecules at time t; this is also the surface density of isolated CO_2 molecules divided by the density of adsorption sites. Similarly, the coverage of CO_2 clusters with size i is denoted by $C_i(t)$. The total density of CO_2 in clusters divided by the density of adsorption sites is $\sum_{i>1} iC_i(t)$. In the simulation we consider i up to 4. We therefore have the following rate equations:

$$\frac{{\rm d}C_1(t)}{{\rm d}t} = -(2C_1(t) + C_2(t) + C_3(t))C_1(t)D(t) \quad (3)$$

$$\frac{{\rm d}C_2(t)}{{\rm d}t} = (C_1(t) - C_2(t))C_1(t)D(t) \quad (4)$$

$$\frac{{\rm d}C_3(t)}{{\rm d}t} = (C_2(t) - C_3(t))C_1(t)D(t) \quad (5)$$

$$\frac{{\rm d}C_4(t)}{{\rm d}t} = C_3(t)C_1(t)D(t) \quad (6)$$

Based on this simple rate equation model, we run simulations for the experiment shown in Figure 2. The initial condition of the simulation is taken to be $C_1(0) = 0.23$ and $C_{i>1}(0) = 0$, where 0.23 ML is the initial surface coverage. Figure 10 shows the comparison between experimental and simulation results of the coverage of CO_2 both in clusters and as isolated molecules. The measured coverages are normalized to the coverage 0.23 ML. At above 70 K, CO_2 desorption begins, which is not simulated by the model. It can been seen that $E_{\rm dif} = 2150 \pm 50$ K fits the experimental data well.

We performed a calculation similar to that in Öberg et al. (2009) to predict the segregation temperature $T_{\rm seg}$ at an astrophysical relevant timescale. We assumed three different heating rates of dust grains, 10^{-2}, 10^{-3}, and 10^{-4} K per year, which covers a wider range than in a typical warm-up model. The energy barrier for diffusion is 2150 ± 50 K. We assume that on average it takes each CO_2 molecule 5 diffusion steps to encounter another CO_2 and segregate or form clusters, which is a reasonable estimate considering the CO_2 abundance

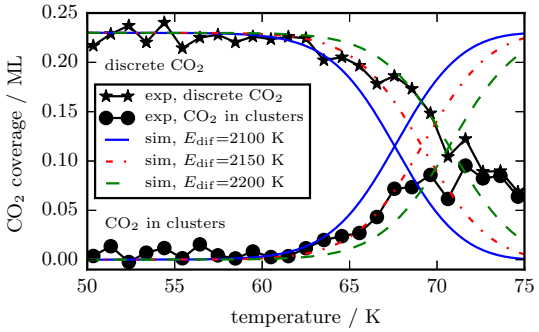

Figure 10. Comparison of measured and simulated amount of CO_2 in clusters and as isolated molecules on np-ASW expressed in units of fractions of a monolayer. The measured amount of CO_2 is obtained from the integration of the two peaks in Figure 2; it is then normalized to the CO_2 coverage. The simulation was performed for three different values of the diffusion energy barrier: $E_{\rm dif} = 2100, 2150, 2200$ K.

with respect to water. It is found that the segregation temperature $T_{\rm seg} = 43 \pm 3$ K. This is higher than the value obtained by Öberg et al. (2009) who assumed a heating rate of 30 K in 4,000 years and a CO_2 concentration of 0.16 in water ice.

In summary, we found that the diffusion energy barrier for a CO_2 molecule diffusing on np-ASW is 2150±50 K, assuming a diffusion prefactor of 10^{12} s^{-1}. A calculation shows that at astrophysical timescales the CO_2 segregation temperature is 43 ± 3 K. This temperature is higher than the one at which there is CO distillation in CO:CO_2 ice (Pontoppidan et al. 2008). Assuming the same prefactor for desorption, we also obtained the binding energies of CO_2 on CO_2 ice and CO_2 on np-ASW to be 2415 ± 20 K and 2250 ± 20 K, respectively. A stronger binding of CO_2-CO_2 than CO_2-H_2O is consistent with the non-wetting of CO_2 on water ice. These values can then be used in simulations of the formation and evolution of mixed ices in the ISM.

5. ACKNOWLEDGMENTS

This research was supported by NSF Astronomy & Astrophysics Division Grants #1311958 and #1615897.

6. APPENDIX

The deposition of CO_2 on np-ASW is obtained either from filling the chamber at a given pressure for a given time (background deposition) or using the molecular beam. The molecular beam deposition is slow and has a narrow angular spread, thus it is targeted to the sample with minimal deposition of CO_2 molecules on other parts of the apparatus. The deposition rate from background R_{bg} can be calculated by

$$R_{bg} = nv/4 \quad (7)$$

$$n = P/k_{\rm B}T \quad (8)$$

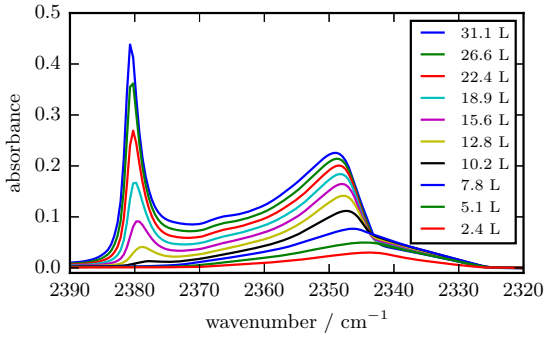

Figure 11. CO_2 ν_3 band during background deposition of CO_2 on 100 L of water ice that is deposited on gold surface at 10 K and warmed to 67 K.

where n is the density in the gas phase, v is the velocity of the gas particle, P is the pressure in the chamber, and T is the gas temperature. The gas pressure was assumed to be homogeneous in the chamber. The gas specific correction factor of ionization gauge was already taken into account. The temperature of the gas was taken to be the same as the chamber wall. The deposition rate from the beam was obtained by comparing the IR of CO_2 deposited from the beam with that from background deposition. In the calibration experiments, CO_2 was deposited on 100 L of water that was deposited at 10 K and warmed to 67 K. At 67 K CO_2 is mobile on the water surface. RAIRS spectra were taken during CO_2 deposition as shown in the Figure 11. At increasing coverage, the 2344 cm^{-1} feature moves to higher wavenumber, while the 2380 cm^{-1} peak begins to emerge (for clarity, only traces at selected exposures are shown). The benchmark coverage was chosen to be the one at which the 2344 cm^{-1} peak is at the same height as the 2380 cm^{-1} peak. This benchmark coverage is independent of deposition method—background and beam deposition. It only depends on the coverage of CO_2 on the part of the water ice that is covered by CO_2. Therefore this is a reliable method to obtain the absolute intensity of the beam. The relative uncertainty of the beam intensity calibration is 5%.

REFERENCES

Al-Halabi, A., Fraser, H. J., Kroes, G. J., & van Dishoeck, E. F. 2004, A&A, 422, 777

Baratta, G. A., Palumbo, M. E., & Strazzulla, G. 2000, A&A, 357, 1045

Bernstein, M. P., Cruikshank, D. P., & Sandford, S. A. 2005, Icar, 179, 527

Berreman, D. W. 1963, PhRv, 130, 2193

Boogert, A. C. A., Gerakines, P. A., & Whittet, D. C. B. 2015, ARA&A, 53, 541

Cook, A. M., Whittet, D. C. B., Shenoy, S. S., et al. 2011, ApJ, 730, 124

Cuppen, H. M., Penteado, E. M., Isokoski, K., van der Marel, N., & Linnartz, H. 2011, MNRAS, 417, 2809

Dartois, E., Schutte, W., Geballe, T. R., et al. 1999, A&A, 342, L32

Edridge, J. L., Freimann, K., Burke, D. J., & Brown, W. A. 2013, RSPTA, 371, 20110578

Ehrenfreund, P., Dartois, E., Demyk, K., & D'Hendecourt, L. 1998, A&A, 339, L17

Ehrenfreund, P., Kerkhof, O., Schutte, W. A., et al. 1999, A&A, 350, 240

Escribano, R. M., Munoz Caro, G. M., Cruz-Diaz, G. A., Rodriguez-Lazcano, Y., & Mate, B. 2013, PNAS, 110, 12899

Gerakines, P. A., & Hudson, R. L. 2015, ApJL, 808, L40

Gerakines, P. A., Whittet, D. C. B., Ehrenfreund, P., et al. 1999, ApJ, 522, 357

Ghesquière, P., Mineva, T., Talbi, D., et al. 2015, PCCP, 17, 11455

He, J., Acharyya, K., & Vidali, G. 2016a, ApJ, 825, 89

—. 2016b, ApJ, 823, 56

He, J., Emtiaz, S., & Vidali, G. 2016, in prep.

Hodyss, R., Johnson, P. V., Orzechowska, G. E., Goguen, J. D., & Kanik, I. 2008, Icar, 194, 836

Ioppolo, S., Palumbo, M. E., Baratta, G. A., & Mennella, V. 2009, A&A, 493, 1017

Ioppolo, S., Sangiorgio, I., Baratta, G. A., & Palumbo, M. E. 2013, A&A, 554, A34

Isokoski, K., Bossa, J.-B., Triemstra, T., & Linnartz, H. 2014, PCCP, 16, 3456

Karssemeijer, L. J., de Wijs, G. A., & Cuppen, H. M. 2014, PCCP, 16, 15630

Keane, J. V., Boogert, A. C. A., Tielens, A. G. G. M., Ehrenfreund, P., & Schutte, W. A. 2001, A&A, 375, L43

Kolasinski, K. 2008, Surface Science: Foundations of Catalysis and Nanoscience (Wiley)

Lauck, T., Karssemeijer, L., Shulenberger, K., et al. 2015, ApJ, 801, 118

Mispelaer, F., Theulé, P., Aouididi, H., et al. 2013, A&A, 555, A13

Noble, J. A., Congiu, E., Dulieu, F., & Fraser, H. J. 2012, MNRAS, 421, 768

Nummelin, A., Whittet, D. C. B., Gibb, E. L., Gerakines, P. A., & Chiar, J. E. 2001, ApJ, 558, 185

Öberg, K. I., Fayolle, E. C., Cuppen, H. M., van Dishoeck, E. F., & Linnartz, H. 2009, A&A, 505, 183

Palumbo, M. E. 2006, A&A, 453, 903

Palumbo, M. E., & Baratta, G. A. 2000, A&A, 361, 298

Palumbo, M. E., Baratta, G. A., Collings, M. P., & McCoustra, M. R. S. 2006, Physical Chemistry Chemical Physics (Incorporating Faraday Transactions), 8, 279

Pontoppidan, K. M., Fraser, H. J., Dartois, E., et al. 2003, A&A, 408, 981

Pontoppidan, K. M., Boogert, A. C. A., Fraser, H. J., et al. 2008, ApJ, 678, 1005

Ratsch, C., & Venables, J. A. 2003, JVST, 21, S96

Whittet, D. C. B., Cook, A. M., Chiar, J. E., et al. 2009, ApJ, 695, 94

Whittet, D. C. B., Shenoy, S. S., Bergin, E. A., et al. 2007, ApJ, 655, 332

Whittet, D. C. B., Gerakines, P. A., Tielens, A. G. G. M., et al. 1998, ApJL, 498, L159